# Si nanopillar arrays with nanocrystals produced by template-induced growth at room temperature*

Bai An-Qi(白安琪), Zheng Jun(郑 军), Tao Ye-Liao(陶冶了), Zuo Yu-Hua(左玉华), Xue Chun-Lai(薛春来), Cheng Bu-Wen(成步文)†, and Wang Qi-Ming(王启明)

*State Key Laboratory on Integrated Optoelectronics, Institute of Semiconductors, Chinese Academy of Sciences, Beijing* 100083, *China*

(Received 8 April 2011; revised manuscript received 29 June 2011)

Well-aligned and closely-packed silicon nanopillar (SNP) arrays are fabricated by using a simple method with magnetron sputtering of Si on a porous anodic alumina (PAA) template at room temperature. The SNPs are formed by selective growth on the top of the PAA pore walls. The growth mechanism analysis indicates that the structure of the SNPs can be modulated by the pore spacing of the PAA and the sputtering process and is independent of the wall width of the PAA. Moreover, nanocrystals are identified by using transmission electron microscopy in the as-deposited SNP samples, which are related to the heat isolation structure of the SNPs. The Raman focus depth profile reveals a high crystallization ratio on the surface.

**Keywords:** silicon nanopillar arrays, porous anodic alumina, nanocrystal, room temperature

**PACS:** 61.46.Km, 78.67.Qa, 81.16.Dn, 61.46.Hk **DOI:** 10.1088/1674-1056/20/11/116103

## 1. Introduction

Semiconductor nanostructures have shown unique electrical, optical and mechanical properties resulting from their quantum dimensions, which offers us new approaches to realizing new functions in electronic and optical devices.[1−8] For example, Si-based nanostructures may challenge the nature of the indirect bandgap via the quantum confinement effect and thus become potential candidates for efficient light emitting devices.[3,4] Semiconductor nanopillar arrays have been used in solar cells to improve the light absorption and the carrier collection efficiency.[5,6] However, the fabrication of semiconductor nanopillar and nanowire arrays usually suffers from technological limitations, such as high temperature, complicated fabrication procedures[9] and unfavourable structural properties.[6]

Here we report a novel method for fabricating Si nanopillar (SNP) arrays, utilizing the porous anodic alumina (PAA) on a substrate as the template and the Si selective deposition by the magnetron sputtering. We prepare SNP arrays with a high order. The method is tolerant of irregularity of the template, has a large filling factor and has controllable structural parameters. The SNP–PAA structure can be prepared on any substrate, such as Al, Si and quartz. Moreover, the microstructure investigations reveal that the Si nanocrystals are formed in the SNPs during the deposition process using the magnetron sputtering at room temperature.

## 2. Experimental method

The fabrication method is very simple, consisting of the two steps illustrated in Fig. 1. First, an ultrathin (100–300 nm) PAA membrane was obtained. The preparation of the PAA membrane was carried out with a two-step anodization (4wt.% oxalic acid solution, 40 W, 20 °C) of an Al foil or an Al film (2-μm thick) evaporated on a substrate (Si or quartz). The employment of the two-step anodization was to reduce the thickness of the membrane and to improve the regularity of the pores to a certain extent.[10] Second, an Si film was deposited on the PAA membrane by using the radio frequency (RF) magnetron sputtering (125 W, 2–4 h) with an Si target in the atmosphere of Ar (3 mTorr) at room temperature. The growth rate was 0.26 Å/s. The chamber base pressure was less than $4\times10^{-5}$ Pa before the deposition. During the deposition, the substrate was rotated at 10 rpm to guarantee a good film uniformity across the surface.

*Project supported by the Major State Basic Research Programme of China (Grant No. 2007CB613404), the National Natural Science Foundation of China (Grant Nos. 60906035, 61036001, 61036003, and 51072194), and the Knowledge Innovation Program of the Chinese Academy of Sciences (Grant No. ISCAS2009T01).

†Corresponding author. E-mail: cbw@semi.ac.cn

© 2011 Chinese Physical Society and IOP Publishing Ltd

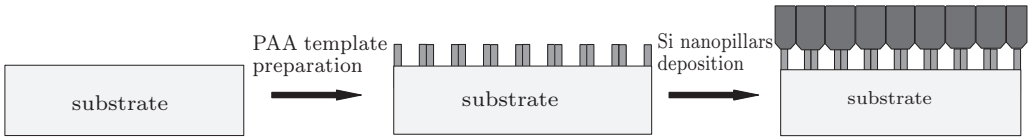



**Fig. 1.** Schematic diagram of the fabrication process.

## 3. Results and discussion

Figure 2 shows the scanning electron microscopy (SEM) images of the SNP arrays. Here, two kinds of samples were prepared. One sample was based on the PAA anodized from an Al foil and had the SNPs–PAA–Al structure. The other sample was based on the PAA anodized from the Al evaporated on an Si substrate and had the SNPs–PAA–Si structure. Figures 2(a) and 2(b) show the oblique angle images of the SNPs–PAA–Al structure. It can be seen that the Si sputtered particles are not deposited into the PAA pores, since the sputtering in the $10^{-1}$ Pa range of pressure does not tend to produce conformal coatings on the substrate with nanoscale high-aspect ratio features. Instead, a nanopillar structure with a height of 95 nm and a diameter of about 80 nm is produced on the top of the PAA pore walls. The fissures between the SNP arrays are attributed to the bend of the elastic Al foil substrate. Figures 2(c) and 2(d) show the cross-sectional and the top view images of the SNPs–PAA–Si structure. Similar nanopillars each with a height of 325 nm and a diameter of 84.3 nm are shown. In both the two structures, the SNPs are arranged hexagonally, well-aligned and closely-packed with a large filling factor of more than 90%. It should be noticed that even some of the PAA walls are not perfectly arranged as shown in Fig. 2(c), the SNPs on the top of them also possess an uniform configuration and arrangement.

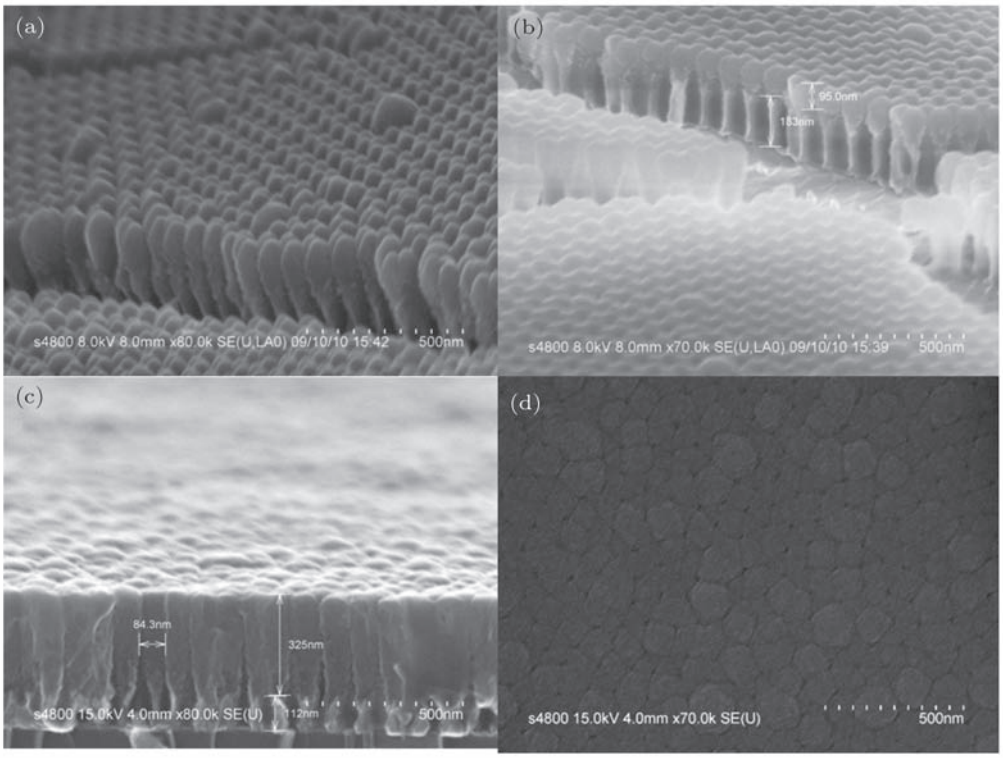



**Fig. 2.** (a) and (b) SEM images of SNPs–PAA–Al structure , (c) cross-sectional and (d) top view SEM images of SNPs–PAA–Si structure.

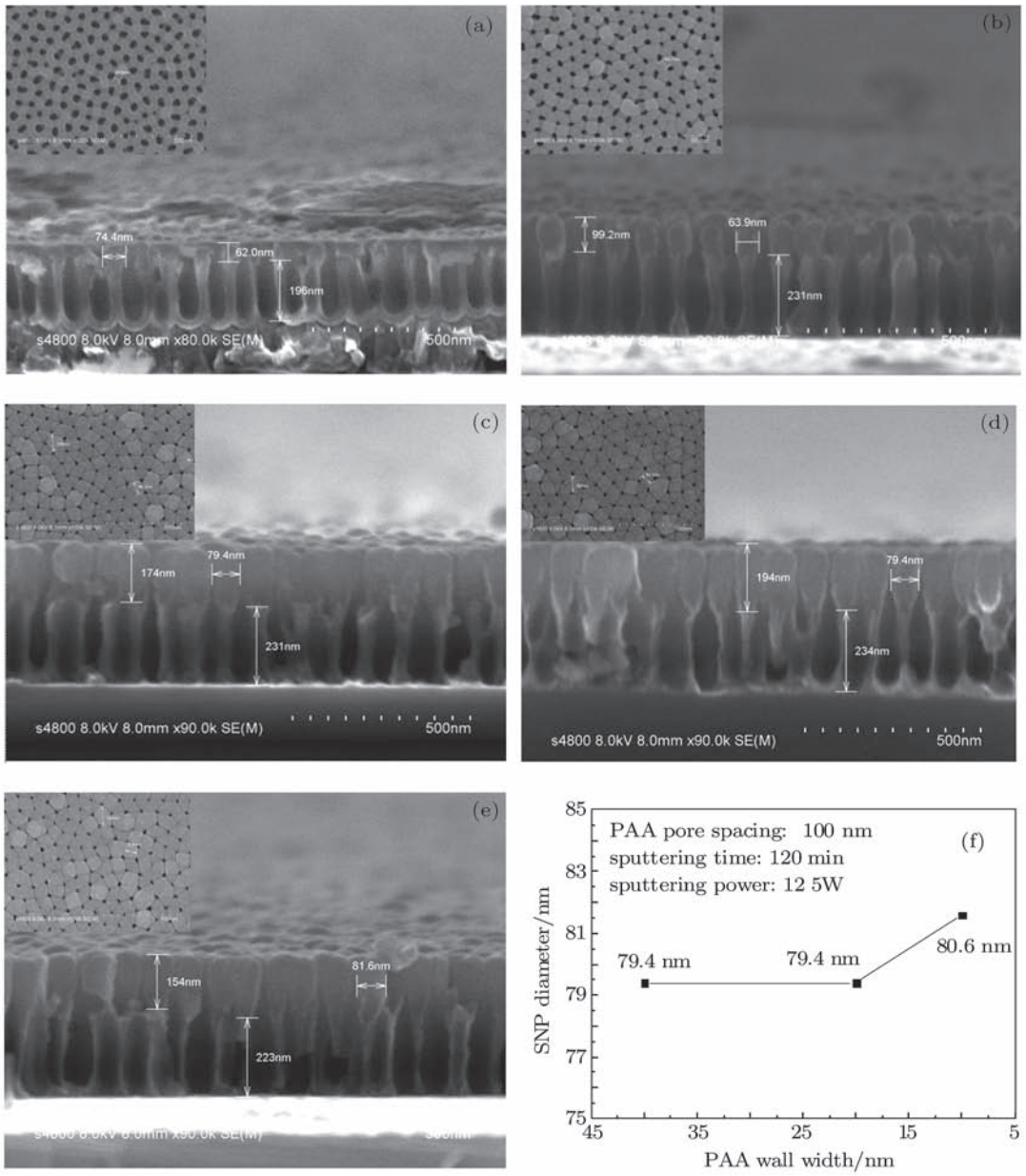



**Fig. 3.** SEM cross-sectional images of SNPs with sputtering power of 125 W at room temperature and sputtering times of (a) 30 min, (b) 60 min and (c) (d) (e) 120 min. The pore wall widths of PAA templates are 40 nm in (a), (b) and (c), 20 nm in (d) and 10 nm in (e). The corresponding top view images are shown in the inserts. (f) Evolution of SNP dimeter as a function of PAA wall depth.

In order to obtain more information about the nanopillar growth and the structural properties, the configurations of the SNPs at different growing stages were obtained using the SEM and are shown in Figs. 3(a)–3(c). The images were obtained after sputtering for 30 min, 60 min and 120 min at 125 W. It is shown in Fig. 3(a) that the surface on the top of the PAA is flat (see the cross-sectional view) and the material distribution is continuous (see the top view), although there are already some islands appearing on nodes of the PAA pore walls. Then in Fig. 3(b), obvious undulations in the cross-sectional view and bounds between the pillars in the top view can be identified. With the pillars growing, the bounds become more evident as shown in Fig. 3(c). From Figs. 3(a)–3(c), it can be deduced that the Si particles sputtered are first deposited entirely on the top of the PAA walls. Afterwards, the Si growth at the skeleton nodes has an advantage, which may be due to the predominant nucleation at the nodes. The nanopillars grow longitudinally and horizontally at the same time, which means that the diameters and the heights of the SNPs

can be controlled by the sputtering process. The PAA-structure-dependent SNP configurations are shown in Figs. 3(c)–3(e), which were obtained after the same sputtering process. The PAA templates shown in Figs. 3(c)–3(e) have the same pore spacing but different wall widths. With the nanopillars growing, the diameters of the nanopillars shown in Figs. 3(c)–3(e) become approximately uniform (79.4–81.6 nm) as shown in Fig. 3(f). Apparently the structural parameters of the SNPs are determined only by the sputtering process and the pore spacing of the PAA.

The crystallinity of the SNP was studied by using the high resolution transmission electron microscopy (HRTEM). The image is shown Fig. 4(a), in which more than one nanocrystal can be identified, although most of the pillars are amorphous Si. The diameters of the nanocrystals approximately range from 2 nm to 5 nm. The composition of the nanocrystals was qualitatively confirmed by the energy-dispersive X-ray spectroscopy (EDX). The highly pure Si can be identified (Fig. 4(b)). By the former experiences, the formation of the crystalline Si by sputtering requires specific conditions,[11−13] such as a high substrate temperature (> 450 °C),[11] a high sputtering power,[12] and thermal treatments after the sputtering,[13] so it is remarkable for us to find the crystalline Si after the sputtering at room temperature without any thermal treatment. The crystallization is considered to be caused by the peculiar structure of the SNPs, which leads to the rise of the local temperature resulted from the energy conversion of the sputtered particles. Different from the case of the bulk material, the nanometer dimensions of the SNPs strongly restrict the heat diffusion, making them good heat isolation structures with a low thermal conduction. The thermal conduction ($G$) of the nanopillars can be derived as

$$G = k\frac{A}{L}, \tag{1}$$

where $k$ is the thermal conductivity coefficient of the material, $A$ is the area of the thermal conduction and $L$ is the length of the thermal conduction. For example, the diameter and the length of the SNP shown in Fig. 2(c) are 84 nm and 325 nm, respectively and $k$ of Si is 1.40 W/cm·K, so $G$ of the SNP is $1.70\times10^{-6}$ W/K, which is several orders of magnitude smaller than that of the bulk Si. Moreover, as the nanopillars grow, the value of $A/L$ becomes even smaller and the thermal conduction on the surface becomes even lower. Consequently, the distinctly low thermal conduction leads to the high heat energy collection at the sample surface, which induces the crystallization.

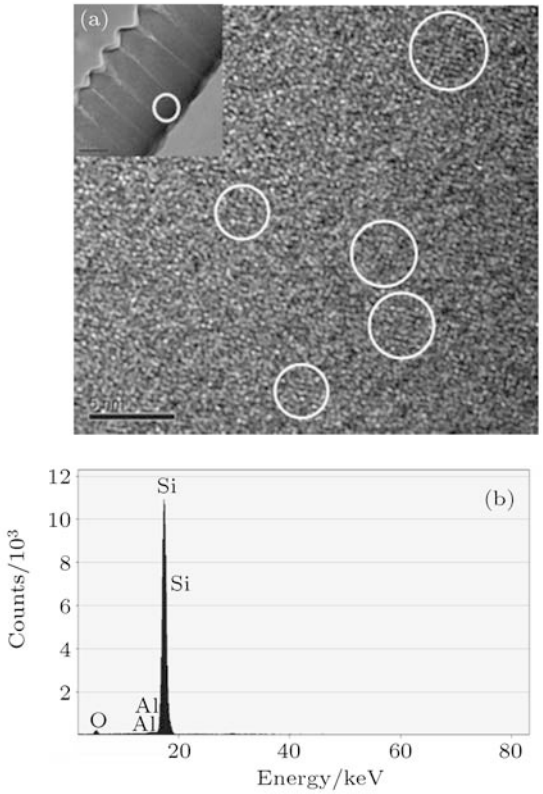



**Fig. 4.** (a) HRTEM cross-sectional image of the SNP, which is obtained in the region showed in the insert. The white circles show the nanocrystals. (b) EDX results of the SNP.

Further, the optical investigation of the SNPs using the micro-Raman spectroscopy was carried out. Figure 5 shows a set of Raman spectra of the SNPs–PAA–Al structure. The Raman spectra from top to down in Fig. 5 correspond to the increasing focus depth, that is, from surface to inner material, in other words, opposite to the growth direction. The exponentially reduced spectrum intensities are generated from the enhanced absorption of the upper material. In the growth direction, the evolvement of the Raman characteristic peak from the a-Si to the crystalline Si is shown clearly, i.e., the a-Si peak at 480 $cm^{-1}$ becomes weakened and subsequently vanishes, at the same time the crystalline Si peak shows up and becomes enhanced. The Raman spectrum at the surface indicates a high crystallization ratio. The evolution shows that at the beginning of the growth, the silicon is amorphous, as the SNPs grow, the nanocrystals form and become denser. The evolution is consistent with our analysis that as the SNPs grow, the reduction of the

thermal conduction leads to the collection of the heat energy and hence facilitates the crystallization process. Similar results of Raman spectra were obtained from samples on Si and $SiO_2$ substrates (SNPs–PAA–Si and SNPs–PAA–$SiO_2$ structures), which excluded the influence of the substrate on the Raman spectra.

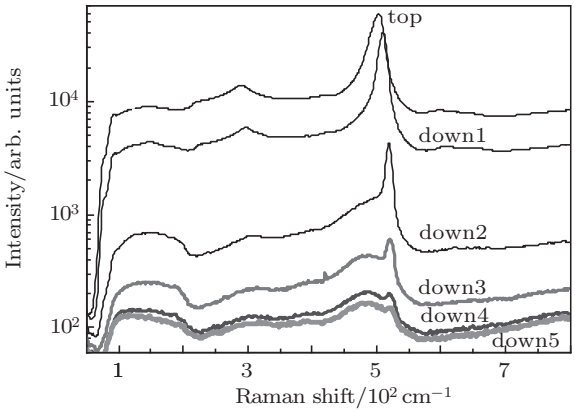



**Fig. 5.** Raman spectra obtained by varying focus depth. The spectra from top to down correspond to the increasing focus depth.

It is also noticed that the crystalline Si peak initially at about 520 $cm^{-1}$ shifts toward the lower energy as the focus depth reduces. The determinant of the red shift is considered to be the rising temperature in the observation area caused by the laser irradiation and the heat isolation structure of the SNPs. The upper focus means the more laser power reaching. We confirm the above analysis by examining the laser power dependence of the Raman spectra, which is shown in Fig. 6(a). With the incident laser power increasing from 3 mW to 20 mW, the crystalline Si peak shifts from 516 $cm^{-1}$ to 498 $cm^{-1}$, which means a red shift of 18 $cm^{-1}$. Similar analyses are made after Si has been sputtered onto the plane substrate and shown in the insert. A comparison shows that the typical a-Si Raman peak is revealed with a corresponding red shift of 7 $cm^{-1}$. Evidently, the red shift for the nanopillars is larger than that for the a-Si because of the heat isolation structure of the nanopillars, which also validates the material discreteness.

In order to exclude the laser heating effect, the laser power is further reduced to obtain the results shown in Fig. 6(b). With the laser heating effect weakened, the crystalline Si peak shifts back to 520.4 $cm^{-1}$, which is consistent with TO and LO phonon peaks of the bulk crystalline Si. This is not in agreement with the TEM observation result, since the quantum size of the nanocrystals will cause a red shift of the Si crystalline Raman peak to deviate from 520 $cm^{-1}$. However, besides the laser heating and the quantum size, there are still other factors that can cause the frequency shift, e.g., the compressive strain can induce a blue shift of the Si crystalline Raman peak. A similar obvious compressive strain has been found in the samples grown on a sapphire at a high growth temperature.[14] The strain here may be due to a similar reason, i.e., the thermal mismatch between the alumina template and the Si nanopillar. The smaller thermal expasion coefficient of the SNP induces a residual compressive strain during the cooling stage after the sputtering.

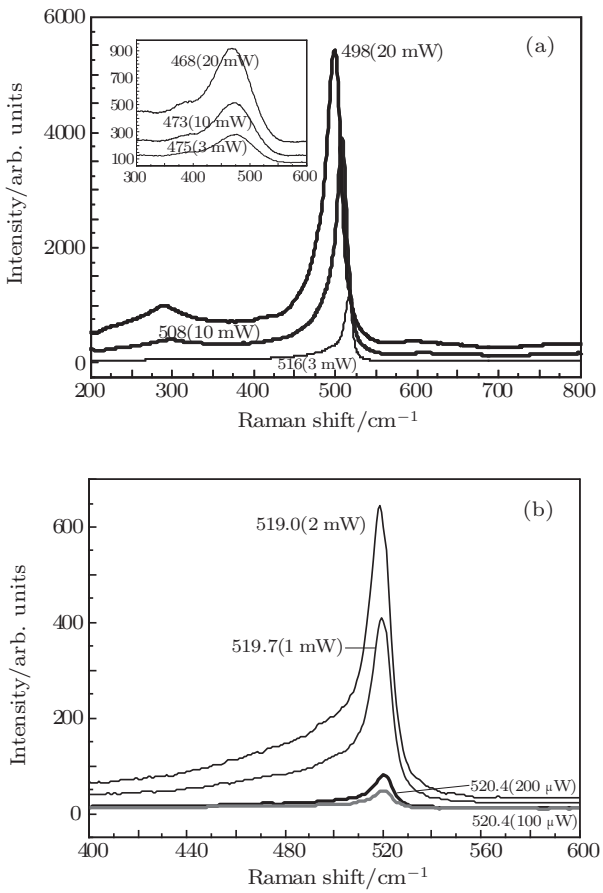



**Fig. 6.** (a) Raman spectrum evolution with the decreasing laser power, the case of a-Si sputtered at plane substrate is shown in the insert for comparison. (b) Raman spectrum evolution with the laser power further decreasing.

# 4. Conclusion

A new method for fabricating SNP arrays on the PAA at room temperature and their fancy configurations and characteristics are reported. The SNPs are concluded to form from the induced growth of the sputtered Si on the top of the PAA skeleton nodes. The structural properties are determined by the pore

spacing of the PAA and the sputtering condition. Moreover, nanocrystalline characteristics are identified in the SNPs through the TEM observation. The poor thermal conduction of the SNP structure is considered to be the main reason for the crystallization, which is then confirmed by Raman spectrum investigations. The Raman focus depth profile reveals an obvious red shift trend of the crystalline Si peak as the SNPs grow, which is attributed to the heat collection of the SNPs from the laser irradiation. Those properties and the fabricating process make the SNP arrays prepared be a competent candidate for realizing novel optoelectronic devices, such as efficient Si based light emitting devices and solar cells.

# References


[1] Brus L E and Trautman J K 1995 *Phil. Trans. R. Soc. Lond.* A **353** 313

[2] Alivisatos A P 1996 *Science* **271** 933

[3] Wang Q M 2002 *Prog. Phys.* **22** 359 (in Chinese)

[4] Cloutier S G, Kossyrev P A and Xu J 2005 *Nat. Mater.* **4** 887

[5] Fan Z Y, Razavi H, Do J W, Moriwaki A, Ergen O, Chueh Y L, Leu P W, Ho J C, Takahashi T, Reichertz L A, Neale S, Yu K, Wu M, Ager J W and Javey A 2009 *Nat. Mater.* **8** 648

[6] Garnett E and Yang P D 2010 *Nano Lett.* **10** 1082

[7] Kan P Z, Zhao S L, Xu Z, Kong C, Wang D W and Yan Y 2010 *Acta Phys. Sin.* **59** 616 (in Chinese)

[8] Bai A Q, Hu D, Ding W C, Su S J, Hu W X, Xue C L, Fan Z C, Cheng B W, Yu Y D and Wang Q M 2009 *Acta Phys. Sin.* **58** 4997 (in Chinese)

[9] Tian B Z, Zheng X L, Kempa T J, Fang Y, Yu N F, Yu G H, Huang J L and Lieber C M 2007 *Nature* **449** 885

[10] Bai A Q, Cheng B W, Wang X F, Xue C L, Zuo Y H and Wang Q M 2010 *J. Nanosci. Nanotechnol.* **10** 7428

[11] Motta N, Rosei F, Sgarlata A, Capellini G, Mobilio S and Boscherini F 2002 *Mater. Sci. Eng.* B **88** 264

[12] Goncalves C, Charvet S, Zeinert A, Clin M and Zellama K 2002 *Thin Solid Films* **403** 91

[13] Silalahi S T H, Yang H Y, Pita K and Yu M B 2009 *Electrochem. Solid-State Lett.* **12** K29

[14] Zuo Y H, Tao Y L, Zheng J, Cao Q, Ma Z H, Wang W, Xue C L, Zhang G Z, Cheng B W, Wang Q M and Xu J 2010 *25th European Photovoltaic Solar Energy Conference and Exhibition,* September 6–10, 2010 Valencia, Spain, poster 1.DV.3.70